Observations of highly regular oscillations in the overflow plume downstream of the Faroe Bank Channel

F. Geyer[1,2,3], S. Østerhus[3,1], B. Hansen[4], D. Quadfasel[5]

[1]Geophysical Institute, University of Bergen, Bergen, Norway

[2]Nansen Environmental and Remote Sensing Center, Bergen, Norway

[3]Bjerknes Center for Climate Research, Bergen, Norway

[4]Faroese Fisheries Laboratory, Torshavn, Faroe Islands

[5]Zentrum für Meeres- und Klimaforschung, University of Hamburg, Hamburg, Germany

Florian Geyer

Nansen Environmental and Remote Sensing Center, Thormølensgate 47, N-5006 Bergen, Norway, e-mail: florian.geyer@nersc.no

Svein Østerhus

Bjerknes Center for Climate Research and Geophysical Institute , Allégt. 70, N-5007 Bergen, Norway, e-mail: ngfso@uib.no

Bogi Hansen

Faroese Fisheries Laboratory, P.O.Box 3051, FO-110 Torshavn, Faroe Islands, e-mail: bogihan@frs.fo

Detlef Quadfasel

Universität Hamburg, Zentrum für Meeres- und Klimaforschung, Institut für Meereskunde, Bundesstr. 53, D-20146 Hamburg, Germany, e-mail: quadfasel@ifm.zmaw.de

Abstract

The Faroe Bank Channel (FBC) is the deepest connection between the Atlantic Ocean and the Nordic Seas. This work describes the dynamic properties of the plume of dense overflow water descending from the Faroe Bank Channel using time series data for velocity and temperature from a network of 25 moorings deployed west of the Faroe Bank Channel between July 1999 and February 2001. The cold water plume was identified using mean velocity and temperature data. A regular pattern of strong velocity and temperature oscillations with 88±4 hours period was the most striking feature observed in the FBC overflow plume. These oscillations are initiated in a region where observations indicate supercritical conditions and compare well to recent model results for the FBC overflow plume by Ezer (2006).

1. Introduction

Cold, dense water from the Nordic Seas flows over the system of ridges between Greenland and Scotland eventually to form part of the North Atlantic Deep Water. Thus the exchange of water across the Greenland-Scotland ridge is a fundamental component of the Meridional Overturning Circulation. For a short summary of the Meridional Overturning Circulation and the Overflow over the Greenland-Scotland ridge, see [*Hansen et al.*, 2004]. The overflow is concentrated at the deep straits across the Greenland-Scotland ridge, the deepest of them being the Faroe Bank Channel (FBC, Figure 1). Approximately 2Sv (1 Sv = 10^6 m^3/s) of dense overflow water go through the FBC and then descend as a bottom-trapped plume into the deep Atlantic Ocean [*Østerhus et al.*, 2001]. For a review of observations and theoretical studies of the Faroe Bank Channel overflow see [*Borenäs and Lundberg, 2004*]. The most recent results of ship-based hydrographic and velocity measurements are presented by *Mauritzen et al.* [2005]. The overflow descends with a speed up to 1 m/s, thereby entraining adjacent water masses. The properties of the produced North Atlantic Deep Water therefore strongly differ from the original deep water produced in the Nordic Seas. Most ocean models use parameterizations for overflow plumes, see [*Alendal et al.*, 1994] for an example. Increasing data coverage during the last years shows high flow variability downstream of the Faroe Bank Channel [*Høyer and Quadfasel*, 2001]. The cold overflow plume appears to break up into boluses of cold water [*Hansen and Østerhus*, 2000] with a vertical extension of about 200 m (Figure 2). In the Høyer and Quadfasel study the results had been interpreted as meso-scale eddies similar to those observed in the Denmark Strait outflow.

[Figure 1, Figure 2]

Data from an extended array of current meter moorings covering the Faroe Bank Channel Outflow provided the opportunity to study the time behaviour of the overflow plume in detail. The following section presents the available data; section 3 gives an overview over the different methods used to analyse the data, which are power spectra, singular spectrum analysis and wavelet analysis. Section 4 presents the results of the data analyses: Mean properties of the velocity and temperature data are used to determine the topographic extension of the dense water plume (section 4.1). Strong velocity oscillations as shown in a typical velocity profile motivate the extensive investigation of the dynamic plume behaviour (section 4.2). Section 5 contains a discussion of the plume structure and comparisons to recent model [*Ezer*, 2006] and laboratory [*Cenedese et al.*, 2004] experiments. Finally, section 6 summarizes the main results of this work.

2. Data

A network of 25 moorings (Figure 1) was in operation west of the Faroe Islands between July 1999 and February 2001 to measure bottom currents in the outflow of the Faroe Bank Channel. The moorings were deployed in 3 groups, termed A, B, and C, with different deployment times (Table 1). Thus direct comparisons of results are only possible within these groups. As seen in Figures 2 and 3, the depth of the channel remains relatively constant, less than 900 m, some 25 km northwestwards from the sill to the area where the channel exits into the Iceland Basin. Three of the B moorings (B8, B9, and B10) were located in this region in addition to the mooring at the sill (NWFB). The rest of the B moorings were located in the very steeply sloping region, just west of the channel exit. The A moorings were on a north-south line about a 100 km west of the exit with depths exceeding 1300 m and the C moorings were about 200 km west of the exit where the bottom depth had increased to more than

1500m. The area covers the bottom-trapped plume of cold dense water from the Nordic Seas that traverses the Faroe Bank Channel to descend into the deep North Atlantic Ocean.

[Table 1]

Except for the sill mooring, each mooring was equipped with an RCM8 Aanderaa current meter. Most of the moorings also included a Seabird Microcat CTD. The instruments were situated 5 to 6 meter above bottom for the B moorings and 25 to 30 meters for the A and C moorings. The data from these moorings is the main source for this investigation. In addition, data from an upward-looking Acoustic Doppler Current Profiler (ADCP) deployed at the bottom of the Faroe Bank Channel as part of the EU project VEINS (Variability of Exchanges in the Northern Seas) was used [*Hansen et al.*, 2001]. The lowest data bin at 770 meter depth, that is 42 meter above bottom, was used for comparison with the current meter data. Additional data was provided by a section of CTD-measurements at the exit of the channel from a survey of RV Poseidon in September 2003.

Velocity data from stations B4 and B5 (Figure 2) was not usable due to current meter malfunction. Velocity data from station A4 was distorted by impeded turning of the instrument with respect to the current direction. Therefore velocity data from station A4 was only usable in terms of its time dependency (e.g. to determine the oscillation frequency), but not with regard to amplitude-related information, which also includes current direction.

3. Methods

Power spectrums obtained by windowed Fourier analysis were used to identify stations with significant meso-scale oscillations of about 3.5 days period. The criterion was that the spectral peak had to be sharp and statistically significant with respect to both linear

(representing the turbulent cascade) and 5th order logarithmic background fits (representing any smooth background signal). For the windowed Fourier analysis the time series were split into 3 sections, the mean value of each section was subtracted. The sections were windowed by a Hanning window, which allowed the sections to overlap by half the section length. Then the analysis for each section was carried out and the resulting spectral estimates were averaged. This configuration allowed for good frequency resolution and sufficient reliability of the resulting spectra.

Stations with significant 3.5-day meso-scale oscillation were then further analysed using singular-spectrum analysis (SSA). Singular-spectrum analysis is a model-free algebraic method for analysis of time series. Its aim is to split a time series into different additive components. Typically these components can be interpreted as 'trend' components (that is, smooth and slowly varying parts of the series), various 'oscillatory' components (perhaps with varying amplitudes) and 'noise' components. Detailed information about singular-spectrum analysis (SSA) can be found in *Golyandina et al.* (2001). In this study SSA has been used as a data filter to obtain separate trend and oscillation modes for the time series. The filtering properties of the SSA method proved to be significantly better than simpler methods, for example a running mean filter.

Wavelet analysis was used to investigate the stability of the oscillations with time and to detect changes of oscillation frequency and strength during the investigation period. The wavelet transform is done by convolution of the time series with a scaled version of the chosen basis function (wavelet) as described in *Torrence and Compo*, (1997). The wavelet chosen for this work was the Morlet wavelet, which is a (complex) plane wave modulated with a Gaussian. The wavelet transform is also complex in this case and the wavelet power spectrum is defined as the squared absolute value of the wavelet transform. It is normalised by the variance of the time series and therefore gives the ratio of signal to (white) noise.

4. Results

4.1. Extension of the FBC overflow plume

Mean current and temperature data from the 25 current meter moorings was used to identify the extension of the cold-water overflow plume. Figure 3 shows the main current system of the Faroe Bank Channel outflow as measured in this campaign, with the mean currents mainly following the isobaths. Mean temperatures below 3°C were associated with the plume, following the definition of the overflow water in the Faroe Bank Channel by *Østerhus et al* (2001). Low temperatures generally coincide with high average velocities. The plume width is increasing with distance from the Faroe Bank Channel in agreement to hydrographic sections taken by *Duncan et al.* (2003). The CTD-section for the western exit of the Faroe Bank Channel is shown in Figure 4. The outflowing plume can be clearly identified by its low temperatures. At these stations the plume begins to shift from the trough onto the northern slope. The horizontal temperature gradients are much stronger on the southern than on the northern side of the plume. The effect of this difference will be adressed when discussing the plume structure (Section 5.1).

[Figure 3, Figure 4]

4.2. Overflow plume dynamics

Many of the stations showed velocity variations with amplitudes from 30 cm/s to about 100 cm/s during a meso-scale range (2-5 days). Temperature varied on the same time

scale with temperature changes of 2 to 5°C. Figure 6 (upper panel) shows a typical velocity dataset.

[Figure 5]

Investigations of the spectral power distribution of velocity and temperature revealed that the meso-scale variability is associated with a narrow spectral peak at 83.5 to 88 hours period (Figure 5). This spectral peak was observed in an area extending from the steeply sloping region just west of the channel exit and past the A mooring line some 100 km downstream. Meso-scale variability with a broad frequency distribution was observed at all distances from the channel. Thus stations C1-C8 show meso-scale variability, but not the clear spectral peak observed further upstream. They are briefly discussed at the end of this chapter. A secondary peak with 120 hours period was observed only within 50km distance from the sill. On the whole, meso-scale oscillations were clearly associated with the cold water plume descending from the Faroe Bank Channel. However station A2 did not show the characteristic oscillation peak of the other stations despite being inside the plume. On the other hand, stations B1 and B7 showed increased meso-scale variability despite being outside the plume, though to a less extent than the neighbouring stations inside the plume. Table 2 shows that the absolute spectral power of the prominent meso-scale spectral peak is decreasing with distance from the Faroe Bank Channel, while the relative power of the spectral peak to the background is increasing. A similar decrease in absolute values with distance from the FBC was also found for the eddy kinetic energy by *Høyer and Quadfasel* (2001).

[Table 2]

The regular oscillations at stations A3-A7, B2, B3 and B6 with the distinct spectral peak at 83.5-88 hours period, allowed further investigation of the current oscillation at these stations. Using the Singular Spectrum Analysis (SSA) method, an oscillation mode related to the 83.5-88 hour spectral peak was filtered out from the data (Figure 6). Having done that with the velocity components, the obtained data could be used to study the oscillation dynamics in detail to gain information about the amplitude, direction and shape in velocity space for all stations where the oscillation mode was significant. This could be compared with a trend mode filtered out by SSA. The filtered data was also used to obtain exact oscillation periods using the autocorrelation method.

[Figure 6]

Plotting the filtered velocity data in velocity space reveals the elliptical form of the velocity oscillation similar to tidal ellipses (Figure 7). By determining points of maximal velocity and averaging them, the main axes of the velocity ellipse were calculated. The size and orientation of the major axis of the velocity ellipse then are mean amplitude and direction of the velocity oscillation, respectively. Taking the average of the trend mode this can be compared to the mean velocity and direction of the trend.

[Figure 7]

The method described above requires a stable phase relation between the velocity in x and y-direction. As this was not the case for some parts of the dataset, these parts had to be neglected. The neglected parts are the last month of data at stations A3-A7 and the first one and a half months at stations B2, B3 and B6, making up one fourth and one third of the respective datasets. A special case occurred at station B6, where the axis of oscillation

changed during May 2000. Therefore the analysis of that station was split in two parts. With the exception of station B2 the ellipses are elongated with a pronounced major axis (high ratio major axis to minor axis). The minor axis is highly variable. It is therefore justified to identify the major axis of the velocity ellipse as the main axis of the current oscillation.

The oscillation amplitude is decreasing in absolute values with increasing distance from the Faroe Bank Channel but increasing in relative strength compared to the mean velocity (trend component), see Table 3. The oscillation main axis is oriented to the left of the mean current for stations B2, B3 and B6 and to the right for stations A3-A7 (note the different time of deployment for the two groups of current meters). Generally, while the mean current is following the isobaths, the current oscillation has a strong cross-slope component (Figure 8). The mean oscillation amplitudes and directions within the cross-sections change gradually along the section. Note especially the increasing relative angle from station A3 to A7.

[Table 3, Figure 8]

Exact estimates of the oscillation periods are obtained using the autocorrelation function of the filtered velocity oscillation. Having determined a main oscillation axis this information can be used to transform the oscillating velocity components into a main oscillation velocity along the oscillation main axis. This velocity is then autocorrelated with itself using time lag as the variable. The period is then found as the first non-zero maximum of the autocorrelation coefficient. The error estimate for the autocorrelation coefficient was used to obtain an error estimate for the oscillation period. In addition the autocorrelation method was used on the oscillation mode of the temperature data.

The average periods are 88 hours for the current and temperature oscillations and agree within the error estimates (see Table 4). No significant deviations from these oscillation periods are present. The autocorrelation factor for one period time lag increases with distance

from the Faroe Bank Channel indicating an increasingly regular oscillation pattern. In order to clarify the relation between current and interface motions, filtered temperature and current oscillations were cross-correlated with different lags. Table 4 shows the lag at which the correlation coefficient was maximal. For the B moorings, the lags were small, indicating near-simultaneity between high temperature (i.e. low interface) and current in the direction specified. For the A moorings, farther downstream, the analysis, on the contrary, indicated an appreciable lag between strong current oscillations (in the directions specified in Table 3) and temperature.

An idea about signal propagation may be had by cross-correlating current oscillation or temperature between two different moorings from the same deployment period and noting the lag, which gives maximal correlation. The result (Table 5) indicates propagation downstream from B6 to B2 and B3 and propagation downslope from A7 to A3.

[Table 4]

Wavelet analysis was used to study the time-dependent velocity spectrum of the plume. Wavelet diagrams for stations A3-A5 show a strong and persistent oscillation at 60 to 120 hours period (see Figure 9 for station A5). This oscillation is remarkably stable from July 1999 until end of September 1999. Then the oscillation abruptly changes frequency twice and eventually seems to weaken. There are also lower frequency signals and the signature of tides.

[Figure 9]

Station B2, B3 and B6 showed a less distinct oscillation signal and a broader range of frequency variations. The stations even further upstream (B8, B9, B10) show lots of low

frequency activity but no significant oscillation signal with stable period. Station NWFB covered the whole time of deployment for stations A1-A7 and B1-B10. The wavelet spectrum indicates oscillations with about 90 hours period from July to September 1999, but none for the rest of the time series (October 1999 to June 2000).

The current meters C1-C8 were deployed about 200 km downstream of the channel exit. The deployment took place 3 weeks after the recovery of the other current meter moorings. Therefore no simultaneous data from stations further upstream exist for comparison. The velocity data is characterised by variations in a broad range of periods between 80 and 300 hours. There are no clear spectral peaks. Since wavelet analysis did not show any structures either, no further investigation was carried out.

5. Discussion

The most remarkable feature revealed by our observations is the discovery that a large part of the overflow plume is dominated by highly regular oscillations in both temperature and velocity. In the region from the sill to the channel exit, the oscillations are not seen or only as weak and intermittent signals, but they are clearly present already in the very steeply sloping area just west of the exit and extend west of the A mooring line but not to the C moorings. These oscillations are highly regular with narrow spectral peaks and a fixed period (88±4 hours) over a wide area and in different observational periods. The oscillatory motions are approximately rectilinear (Figure 7; Table 3).

[Figure 10]

The temperature oscillations should reflect the motion of the interface between the overflow layer and the warmer waters above with a low temperature indicating a high

interface, i.e. a thick overflow plume (Figure 2). At the B moorings, just west of the channel exit, the small lag between upslope current and temperature (Table 4) indicates that the thickest plume occurs with maximum current downslope.

At the A moorings, in contrast, the thickest overflow plume occurs about 1/3 of a period before maximal downslope current and therefore close to the time of slackest current. This is also seen in Figure 10, which shows the current field in relation to the temperature distribution at section A during a period of 11 days. The two northernmost stations A6 and A7 are dominated by oscillations in north-south direction perpendicular to the mean westward current of the plume. In contrast the oscillation velocity at station A3 (61.65°N) is mainly oriented along the mean current. Here the plume speeds up while a cold water core is passing and slows down in between, when water temperatures are higher (but still in many cases below 3°C). The superposition of the two effects leads to the gradual change in the orientation of the velocity oscillation shown in Figure 8 with its increasing angle between mean velocity and mean velocity oscillation from station A3 to A7. A similar plume structure could also be seen at the section from station B1 to B4. Due to the coarser arrangement of moorings at this section the plume structure was not visible in such detail as in the A1-A5 section.

We can compare our observations to recent results from numerical models [*Ezer*, 2006]. He finds a regime of wave-like regular oscillations in his model of the FBC at roughly 100-200km distance from the FBC sill. Observations of regular oscillations in this study were at 75 to 140km distance from the sill. No regular oscillations were found at 260km (section C), again in accordance to the model results, one might speculate if this section was situated in the transition area to the eddy regime that occur downstream of the area of regular oscillations in [Ezer, 2006] as no clear signatures of passing eddies were found either. His oscillations have a somewhat longer period (~5 days) than we observe, but his model was based on a very idealized topography and a fairly coarse resolution compared to the real width of the channel. Although the lack of more quantitative detail makes direct comparison difficult, the similarity

of his Figures 5a+b to our Figure 10 is striking and indicates that the oscillations in his model are similar to those that we observe.

Ezer (2006) points out the similarity of his model results to the different flow regimes observed in the laboratory by *Cenedese et al.* (2004). The regular oscillations would thus compare to what *Cenedese et al.* (2004) term as the ”wave regime”. They studied the behaviour of a dense current flowing down a sloping bottom in a rotating tank and found that the plume consistently exhibited wavelike behaviour when the internal Froude number was close to or exceeding 1 and the Ekman number is on the order of 1.–Indeed, *Duncan et al.* (2003) deduce that Fr > 1 and Ekman numbers on the order of 1 in a wide area downstream of the channel exit from their observations. The observed oscillating behaviour of the FBC overflow plume thus occurs in the same region of Froude-number/Ekman-number space, where *Cenedese et al.* (2004) observed it in their rotating tank.

The waves observed in the laboratory were found to propagate downslope a bit faster than the current and this seems incompatible with our observations. Our experimental setup is not ideal for studying wave propagation, but the time lag from B6 to B2 and B3 (Table 5) would be consistent with a wave propagating in the mean flow direction with a phase speed of about 30 cm s^{-1}, as seen from a system referenced to the bottom. If the wave propagates in other directions, the phase speed would be smaller. It should also be noted that the flow in the laboratory experiments relate to lower Reynolds numbers (Re < 300) than occur in oceanic flows. There are more laboratory studies that observed waves in overflow layers, e.g. *Lane-Serff and Baines* (1998) and *Etling et al.* (2000). In these studies the occurence of waves in the overflow layers appeared simultaneously with intermediate layer eddies.

Apart from the academic importance of identifying such a clear example of this kind of oscillatory motion in nature, our results may help understanding the role of the FBC overflow in the global ocean circulation. As they pass the sill of the channel, the overflow waters form a fairly homogeneous mass of cold water with bottom temperatures well below

zero. When this water reaches the area off Greenland and meets the other contributors to the North Atlantic Deep Water (NADW), its temperature has increased by more than 3^{o}C by entraining and mixing with ambient waters along the route. As seen in Figure 3, most of this temperature increase occurs already within our study area, which implies some exceptionally strong mixing process.

6. Concluding remarks

A regular pattern of velocity and temperature oscillations with 88±4 hours period is observed to dominate a large part of the Faroe Bank Channel overflow plume. This highly coherent ocsillations occur in a region where observations indicate supercritical conditions and compare strikingly to to recent numerical model results [*Ezer*, 2006]. Further research is needed to understand how the observed kinematic structure influences the mixing in the Faroe Bank Channel overflow. For further field studies it would be desirable to also have information of the varying vertical extent of the plume, e.g. by using thermistor strings in addition to current meters.

Acknowledgements

The authors gratefully acknowledge the assistance of Regin Kristiansen and Karin M. H. Larsen at the Faroese Fisheries Laboratory in mooring preparation and data processing and the expertice of the officers and crew of R/V Magnus Heinason. The authors also want to thank T.Gammelsrød for supervising the thesis that lead to this publication and T.Eldevik for his helpful comments. Most of the instrumentation for the field measurements was funded by a grant from the Danish Research Council. This is publication Nr. Axxx from the Bjerknes Center for Climate Research.

Alendal, G., Drange, H. and Haugan P.M. (1994), Modelling of Deep-Sea Gravity Currents Using an Integrated Plume Model, *The Polar Oceans and their Role in Shaping the Global Environment, Geophysical Monograph 85,* 237-246.

Borenäs, K. and Lundberg, P. (2004), The Faroe-Bank Channel deep-water overflow, *Deep-Sea Research II*, 51, 335-350.

Cenedese, C., Whitehead, J.A., Ascarelli, T.A. and Ohiwa, M. (2004), A dense current flowing down a sloping bottom in a rotating fluid, *Journal of Physical Oceanography*, 34 (1), 188-203.

Duncan, L.M., Bryden, H.L. and Cunningham, S.A. (2003), Friction and mixing in the Faroe Bank Channel outflow, *Oceanologica Acta*, Vol.26, 473-486.

Etling, D., Gelhardt, F., Schrader, U., Brennecke, F., Kühn, G., Chabert d'Hieres, G. and Didelle, H. (2000), Experiments with density currents on a sloping bottom in a rotating fluid, *Dynamics of Atmospheres and Oceans*, 31, 139-164.

Ezer, T. (2006), Topographic influence on overflow dynamics: Idealized numerical simulations and the Faroe Bank Channel overflows, *Journal of Geophysical Research*, *111*, C02002, doi:10.1029/2005JC003195.

Golyandina, N., Nekrutin, V. and Zhigljavsky, A. (2001), Analysis of Time Series Structure: SSA and Related Techniques, *New York: Chapman and Hall/CRC*.

Hansen, B. and Østerhus, S. (2000), North Atlantic - Nordic Seas Exchanges, *Progress in Oceanography*, 45, 109-208.

Hansen, B., Østerhus, S., Quadfasel, D. and Turrel W.R. (2004), Already the day after tomorrow?, *Science,* Vol.305, 953-954.

Hansen, B., Turrell, W.R. and Østerhus, S. (2001), Decreasing overflow from the Nordic seas into the Faroe Bank channel since 1950, *Nature*, Vol.411, 927-930.

Høyer, J.L. and Quadfasel, D. (2001), Detection of deep overflows with satellite altimetry, *Geophysical Research Letters,* Vol.28, No.8, 1611-1614.

Lane-Serff, G.F., and Gaines, P.G. (1998), Eddy formation by dense flows on slopes in a rotating field, *Journal of Fluid Mechanics*, vol. 363, 229-252.

Mauritzen, C., Price, J., Sanford, T. and Torres, D. (2005), Circulation and mixing in the Faroese Channels, *Deep Sea Research*, 52, 883-913.

Østerhus, S., Turrell, W.R., Hansen, B., Lundberg, P. and Buch, E. (2001), Observed transport estimates between the North Atlantic and the Arctic Mediterranean in the Iceland-Scotland region, *Polar Research 20(1),* 169-175.

Torrence, C. and Compo, G.P. (1997), A Practical Guide to Wavelet Analysis, *Bulletin of the American Meteorological Society,* 79(1), 61-78.

Figure 1: Map of the investigations area with mooring positions and CTD-section. Different symbols denote: a) moorings inside the plume, with oscillation (open circles), b) moorings inside the plume, but without oscillation (filled circles), c) stations outside the plume, without oscillations (squares), d) stations with no or faulty data (crosses). A: July-Nov 1999, B: Feb-June 2000, C: July-Nov 2000.

Figure 2: Development of the vertical structure of temperature in the overflow plume over a ten day period, measured at a mooring deployed some 100 km downstream of the Faroe Bank Channel, close to later station B2 (see Figure 1). The mooring, containing three thermistor strings with 11 sensors each, experienced severe knock-downs during periods of high current speeds. The actual sensors depths were calculated using pressure recordings from a Microcat mounted at the top of the mooring.

Figure 3: Mean velocity vectors and mean temperatures at the Faroe Bank Channel outflow.

Figure 4: Temperature distribution of the Faroe Bank Channel Exit section.

Figure 5: Power spectrum diagram of station A3, velocity in u-direction, with linear and 5^{th} order logarithmic fit. The vertical black bar gives the 0.9 confidence interval.

Figure 6: Example of raw velocity data and SSA modes, station A3, velocity u-component. The lower plot shows oscillation mode (solid line) and trend mode (dashed line); the upper plot shows how the sum of oscillation and trend mode (thick black line) fits the raw velocity data.

Figure 7: Station A5, plot of velocity oscillation mode (solid line) with points of maximal velocity (open circles) and comparison to trend mode (dotted line). The thick lines denote the major axis of the velocity oscillation and the mean trend velocity.

Figure 8: Map with station A1-A7 and B1-B7 showing mean velocity and mean oscillation for each station. The western end of the Faroe Bank Channel is at the right edge of the map, depth is increasing towards the lower left corner.

Figure 9: Station A5, velocity v-component, time series and wavelet diagram. Black curves give cones of influence, black contours enclose regions of greater than 95% confidence against a fitted red noise spectrum. The colors denote 11 dual-logrithmic steps from 0.0625 (blue) to 64 (red).

Figure 10: Time-latitude plot of the A1-A7 section with temperatures as colour map (hovmoller diagram) and SSA velocity oscillation mode (sticks), 3 cold cores are visible. For station A4 only temperature data was used (see Section 4.1).

Table 1: Mooring positions, time of deployment and used instruments

station	latitude	longitude	echo depth (m)	Deployed	Recovered	RCM	CTD	ADCP
NWFB	61.4167	-8.2833	812	04.07.1999	19.06.2000			x
B1	61.6363	-9.9167	1206	27.02.2000	19.06.2000	x		
B2	61.7356	-9.9942	1081	27.02.2000	19.06.2000	x	x	
B3	61.8365	-9.9965	926	28.02.2000	19.06.2000	x	x	
B4	61.9375	-10.0005	851	28.02.2000	19.06.2000	x		
B5	61.8002	-9.3995	778	28.02.2000	19.06.2000	x	x	
B6	61.6996	-9.5058	919	28.02.2000	19.06.2000	x	x	
B7	61.6022	-9.5998	1003	28.02.2000	19.06.2000	x	x	
B8	61.649	-9.032	845	28.02.2000	19.06.2000	x	x	
B9	61.75	-8.9491	769	28.02.2000	19.06.2000	x	x	
B10	61.6005	-8.6	866	28.02.2000	19.06.2000	x	x	
A1	61.5179	-10.8338	1264	03.07.1999	05.11.1999	x		
A2	61.5836	-10.8341	1321	03.07.1999	05.11.1999	x	x	
A3	61.65	-10.8334	1294	03.07.1999	05.11.1999	x	x	
A4	61.7167	-10.834	1253	03.07.1999	05.11.1999	x	x	
A5	61.7846	-10.8317	1160	03.07.1999	05.11.1999	x	x	
A6	61.8502	-10.8336	1069	03.07.1999	05.11.1999	x	x	
A7	61.919	-10.8339	1028	03.07.1999	05.11.1999	x		
C1	60.8683	-11.579	1228	09.07.2000	13.02.2001	x		
C2	61.0432	-12.885	1725	09.07.2000	13.02.2001	x		
C3	61.3317	-13.2983	1566	09.07.2000	03.11.2000	x		
C4	61.5674	-13.2506	1521	10.07.2000	03.11.2000	x	x	
C5	61.6838	-13.0998	1461	10.07.2000	03.11.2000	x	x	
C6	61.7971	-12.9468	1279	10.07.2000	03.11.2000	x	x	
C7	61.9156	-12.7874	1204	10.07.2000	03.11.2000	x	x	
C8	62.0342	-12.6368	1084	10.07.2000	03.11.2000	x	x	

Table 2: Period and spectral power density of the characteristic spectral peak between 80 and 90 hours period. Spectral power from station A4 not usable (see chapter 4.1).

station	**period (hours)**	**spectral power density (cm^2/s^2) Hz^{-1}**	**ratio of peak to background density**	**distance from sill**
B6	83.5 ± 3	$7.20*10^8$	6.2	75km
B2	83.5 ± 3	$6.33*10^8$	7.2	100km
B3	83.5 ± 3	$3.60*10^8$	5.3	
A3	88 ± 3	$3.01*10^8$	13.0	140km
A4	88 ± 3	$(0.18*10^8)$	(16.6)	
A5	88 ± 3	$4.65*10^8$	20.8	
A6	88 ± 3	$2.66*10^8$	15.3	
A7	88 ± 3	$2.51*10^8$	27.0	

Table 3: Oscillation direction and comparison to trend, results and standard deviations. All angles follow the compass direction and are referenced to north. The direction of the inclination of the oscillation axis is chosen so as to be on the right of the mean flow when looking downstream. For B6, the period was split into two parts.

station	oscillation main axis amplitude (cm/s)	inclination	minor axis amplitude (cm/s)	trend velocity (cm/s)	Direction (angle to north)	relative angle of oscillation to trend
B6 part 1	57 ± 20	62 ± 14°	23 ± 14	79 ± 11	297 ± 6°	125 ± 15°
B6 part 2	116 ± 9	92 ± 4°	15 ± 14	115 ± 8	295 ± 2°	157 ± 5°
B2	51 ± 11	39 ± 13°	33 ± 15	60 ± 5	277 ± 5°	122 ± 13°
B3	44 ± 13	26 ± 11°	11 ± 7	39 ± 5	277 ± 7°	109 ± 13°
A3	37 ± 7	278 ± 7°	6 ± 3	33 ± 6	250 ± 5°	28 ± 9°
A5	42 ± 7	320 ± 10°	7 ± 4	33 ± 5	281 ± 5°	40 ± 11°
A6	33 ± 5	353 ± 11°	7 ± 4	22 ± 2	291 ± 7°	61 ± 13°
A7	27 ± 10	25 ± 14°	7 ± 4	11 ± 2	293 ± 13°	92 ± 19°

Table 4: Oscillation periods calculated from SSA-filtered velocity and temperature data. As no main oscillation could be defined for station B6, current oscillation periods were calculated separately for u and v components of velocity. Autocorrelation factors for a time lag of one period are given. The last two columns show the lag (in hours) at which the crosscorrelation between current and temperature is maximal and the correlation coefficient at this lag. Except for B6, current is represented by the component in the direction of the oscillation main axis (Table 3). Positive lag indicates that current leads temperature.

station	current oscillation		temperature oscillation		Crosscorrelation	
	period (h)	Autocor.	period (h)	Autocor.	Lag (h)	Crosscor.
B6 (u-component)	90 ± 4	0.498	90 ± 4.5	0.444	+2.0	0.93
B6 (v-component)	88 ± 5	0.34			-15.5	0.87
B2	87 ± 3.5	0.526	88.5 ± 4	0.47	-8.0	0.92
B3	87.5 ± 3.5	0.553	94 ± 5	0.364	-16.5	0.79
A2	---	---	85 ± 3.5	0.51	---	---
A3	87.5 ± 3.5	0.586	86 ± 2	0.739	-39.0	0.77
A4	87.5 ± 3	0.6	87 ± 2.5	0.723	---	---
A5	87 ± 2	0.751	86.5 ± 2	0.799	-30.5	0.82
A6	87 ± 2	0.731	87.5 ± 3	0.51	-29.5	0.54
A7	86.5 ± 2	0.794	---	---	---	---

Table 5. Pairwise crosscorrelation between different moorings in the same deployment period. The table shows the lag (in hours) at which the crosscorrelation is maximal and the correlation coefficient at this lag. Crosscorrelations are computed for the current along the main oscillation axis (Table 3) and for temperature. Positive lag indicates that the first mooring leads the second. The first column shows the distance between the moorings.

Moorings	Distance	Current		Temperature	
	(km)	Lag (h)	R	Lag (h)	R
A3 – A4	7.4	---	---	-4.5	0.97
A3 – A5	15.0	-17.5	0.90	-7.0	0.90
A3 – A6	22.3	-23.0	0.91	-12.5	0.67
A3 – A7	30.0	-20.0	0.84	---	---
B6 – B2	26.1	---	---	+20.0	0.88
B6 – B3	30.1	---	---	+27.5	0.78
B2 – B3	11.1	+15.0	0.93	+8.0	0.84

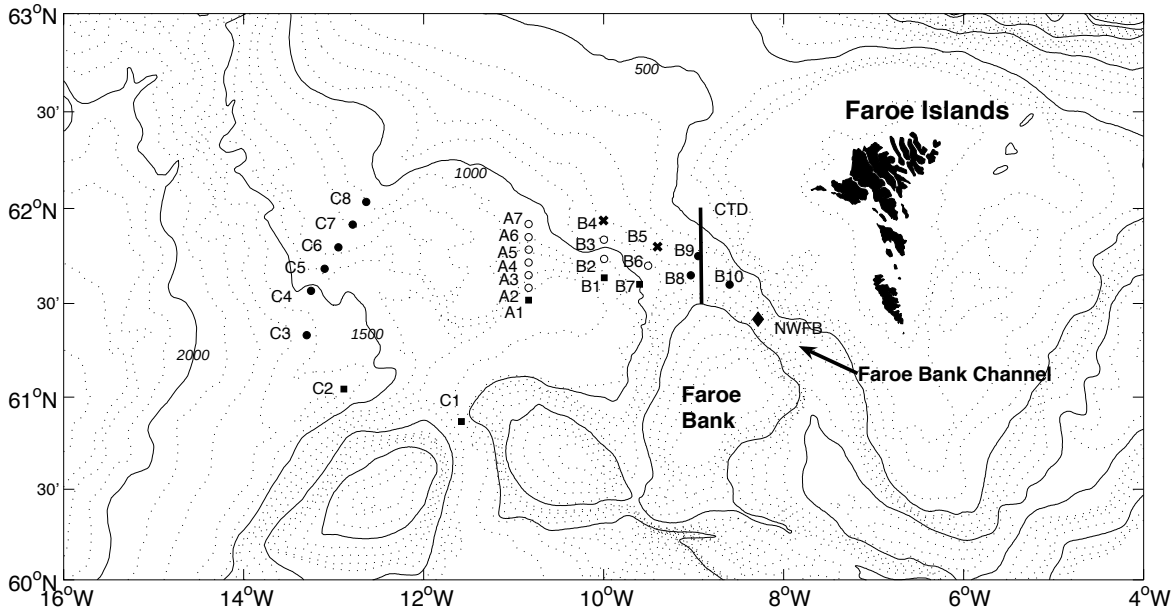
63°N
30'
62°N
30'
61°N
30'
60°N
16°W
14°W
12°W
10°W
8°W
6°W
4°W
500
1000
1500
2000
Faroe Islands
Faroe Bank Channel
Faroe Bank
CTD
NWFB
C1
C2
C3
C4
C5
C6
C7
C8
A1
A2
A3
A4
A5
A6
A7
B1
B2
B3
B4
B5
B6
B7
B8
B9
B10

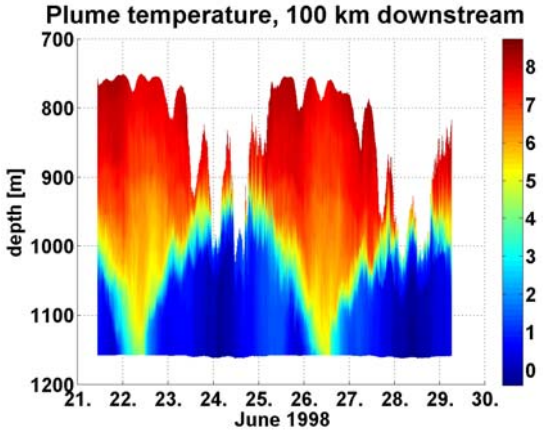
Plume temperature, 100 km downstream
depth [m]
700
800
900
1000
1100
1200
21. 22. 23. 24. 25. 26. 27. 28. 29. 30.
June 1998
8
7
6
5
4
3
2
1
0

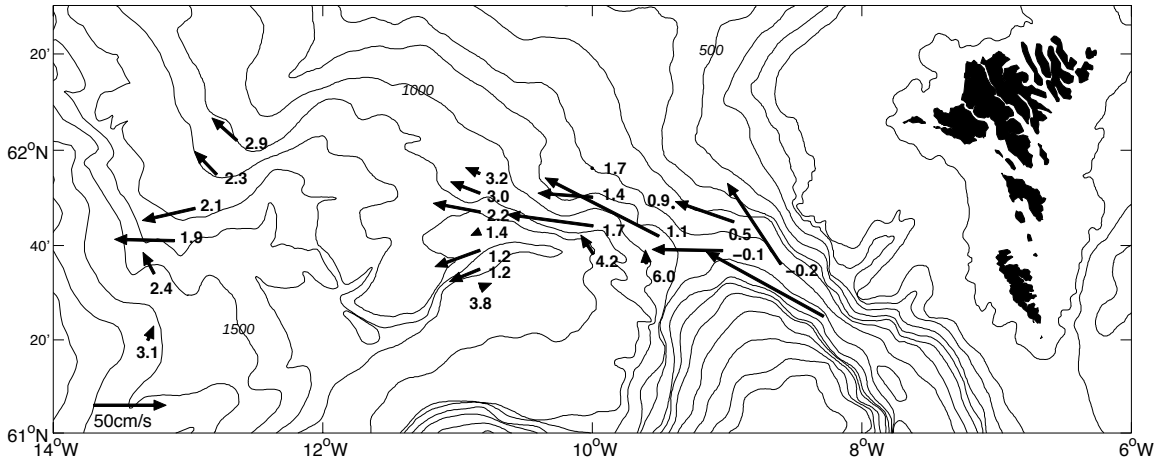
20'
62°N
40'
20'
61°N
14°W
12°W
10°W
8°W
6°W
500
1000
1500
50cm/s
2.9
2.3
2.1
1.9
2.4
3.1
3.2
3.0
2.2
1.4
1.2
1.2
3.8
1.7
1.4
0.9
1.7
1.1
0.5
4.2
−0.1
6.0
−0.2

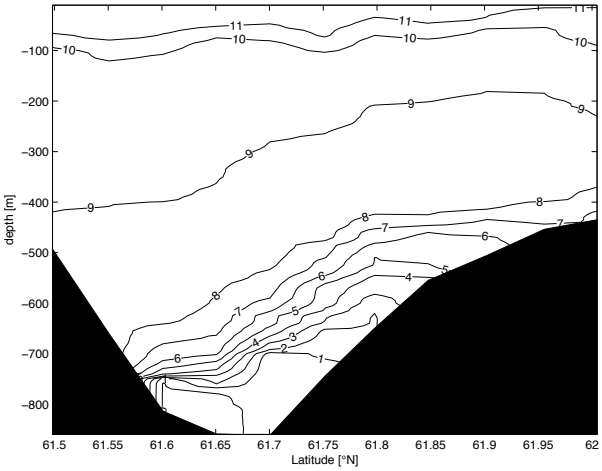
depth [m]
Latitude [°N]

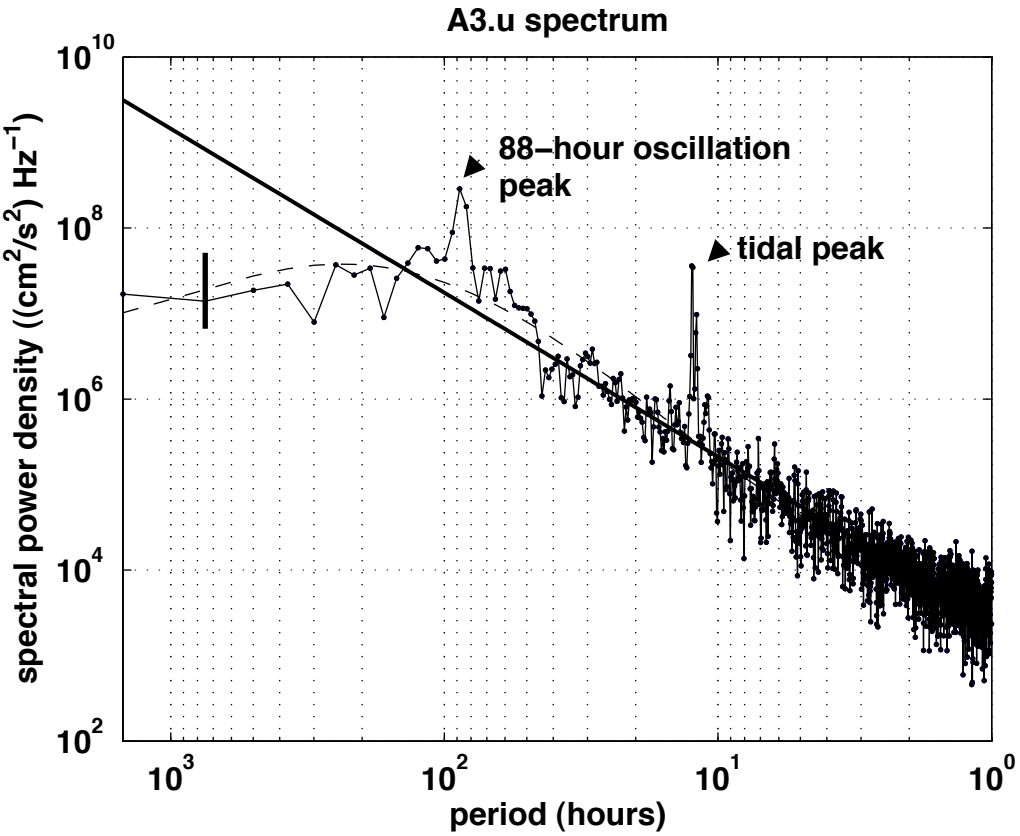
A3.u spectrum
88–hour oscillation peak
tidal peak
spectral power density ((cm²/s²) Hz⁻¹)
period (hours)

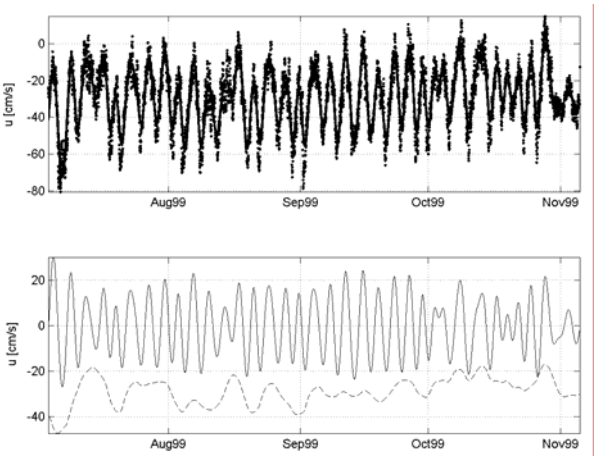
u [cm/s]
Aug99
Sep99
Oct99
Nov99

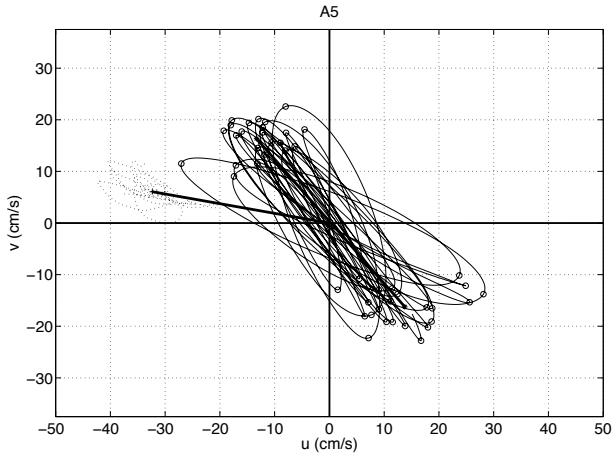
A5
v (cm/s)
u (cm/s)

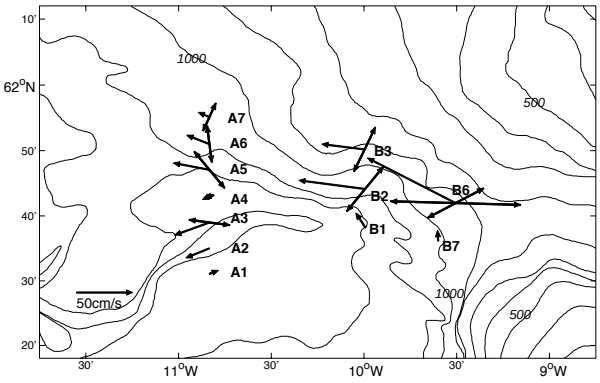
1000
500
A7
A6
A5
A4
A3
A2
A1
B3
B2
B1
B6
B7
50cm/s
62°N
11°W
10°W
9°W

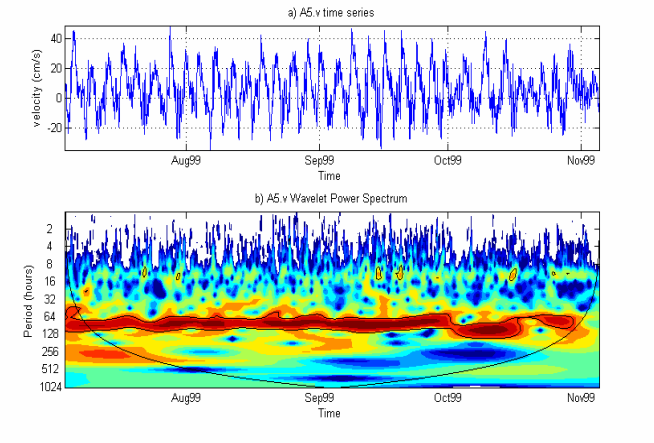
a) A5.v time series
velocity (cm/s)
Aug99
Sep99
Oct99
Nov99
Time
b) A5.v Wavelet Power Spectrum
Period (hours)
Aug99
Sep99
Oct99
Nov99
Time

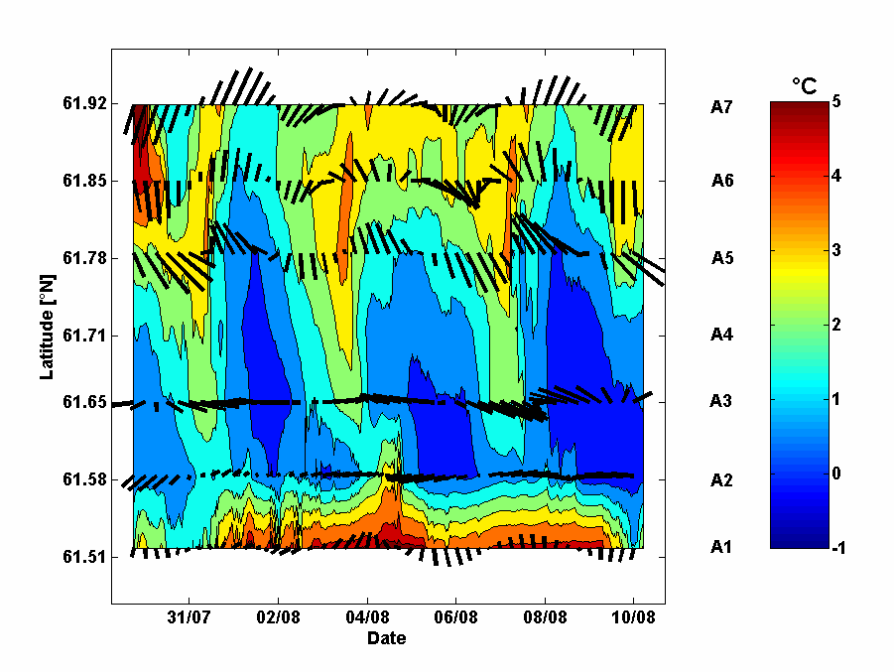
61.92
61.85
61.78
61.71
61.65
61.58
61.51
Latitude [°N]
31/07
02/08
04/08
06/08
08/08
10/08
Date
A7
A6
A5
A4
A3
A2
A1
°C
5
4
3
2
1
0
-1